Bioconjugate Chemistry

Article

pubs.acs.org/bc

Bombesin Peptide Conjugated Gold Nanocages Internalize via Clathrin Mediated Endocytosis

Dhananjay Suresh,[†] Ajit Zambre,[‡] Nripen Chanda,[‡] Timothy J. Hoffman,[∥,¥,§] C. Jeffrey Smith,[‡,∥,⊥] J. David Robertson,[§,⊥] and Raghuraman Kannan*[,†,‡,#]

Departments of [†]Bioengineering, [‡]Radiology, [¥]Medicine and [§]Chemistry, [⊥]University of Missouri Research Reactor, and [#]International Center for Nano/Micro Systems and Nanotechnology, University of Missouri, Columbia, Missouri 65211, United States

[∥]Research Service, Harry S. Truman VA Hospital, Columbia, Missouri 65201, United States

Supporting Information

ABSTRACT: The nature of interaction and mechanism of internalization of receptor-avid peptide nanoparticles with cells is not yet completely understood. This article describes the cellular internalization mechanism and intracellular trafficking of peptide conjugated receptor targeted porous Gold nanocages (AuNCs) in cancer cells. We synthesized and characterized a library of AuNCs conjugated with bombesin (BBN) peptide. Evidence of selective affinity of AuNC-BBN toward gastrin releasing peptide receptors (GRPR) was obtained using radiolabeled competitive cell binding assay. Endocytic mechanism was investigated using cell inhibitor studies and monitored using optical and transmission electron microscopy (TEM). Results show AuNC-BBN uptake in PC3 cells is mediated by clathrin mediated endocytosis (CME). Indeed, in the presence of CME inhibitors, AuNC-BBN uptake in cells is reduced up to 84%. TEM images further confirm CME characteristic clathrin coated pits and lysosomal release of AuNCs. These results demonstrate that peptide ligands conjugated to the surface of nanoparticles maintain their target specificity. This bolsters the case for peptide robustness and its persisting functionality in intracellular vehicular delivery systems.

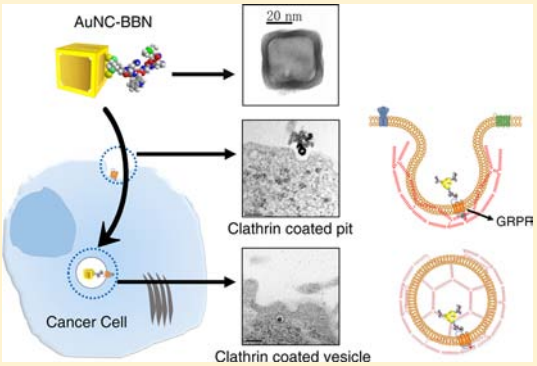

In recent years, nanoparticles have emerged as a promising drug delivery vehicle to transport cytotoxic drugs or genetic materials to cancer cells.[1] The therapeutic efficiencies of these delivery systems depend on two important parameters: (i) the ability to selectively recognize and internalize within a cancer cell and (ii) the ability to release a payload from endosomes to the cancer cell cytoplasm.[2,3] The selective recognition and release factors are governed by mechanisms and molecular processes by which nanoparticles enter and internalize within cells. Indeed, recent observations suggest that the factors such as size, shape, and type of surface ligands on the nanoparticle play a significant role in regulating and modulating cellular interaction processes.[4,5] Nevertheless, a unified mechanism for nanoparticle internalization and consequential understanding of molecular events within the cell has yet to be fully understood.[6−11] Therefore, a study focused on understanding the endocytic mechanism of targeted nanoparticles is vital for the design and development of therapeutically efficient nanoparticle-based delivery systems.

Previous studies demonstrated that functional biomolecules on the surface of nanoparticles play a predominant role in determining the mechanism for internalization: namely, clathrin, caveolae, macropinocytosis or phagocytosis, as shown in Figure 1.[12,13] For example, a recent study showed that gold nanoparticles (AuNPs) functionalized with transferrin enter cells via a clathrin-mediated endocytosis pathway.[14] On the other hand, AuNP surface modified with Cetuximab (C225) antibody alters the internalization pathway to the caveolar mechanism.[15] Furthermore, other studies have shown that morphology of nanoparticles also affects molecular and signaling events of cellular interaction.[16−18] Based upon these experiments, it is evident that the mechanism of endocytosis depends on physicochemical properties, as well as specific functional ligands located on the nanoparticle surface. However, the endocytic mechanisms proposed so far have been limited to nanoparticle surfaces conjugated with either an antibody or small organic molecules.[19−21] To the best of our knowledge, intracellular trafficking studies of receptor-specific peptide conjugated AuNPs in human cancer cells are limited.[22−24] It is worth noting that peptide-based targeting of drug molecules and nanoparticles has shown excellent promise for clinical applications.[25,26] There are several advantages of utilizing a receptor-avid peptide over an antibody for targeted delivery of nanoparticles that include easy mobility, low immunogenicity, and ease of synthesis.[27,28] For example, a 14-amino-acid Bombesin (BBN) peptide demonstrated specif-

Received: July 6, 2014
Revised: July 7, 2014
Published: July 14, 2014

   dx.doi.org/10.1021/bc500295s | *Bioconjugate Chem.* 2014, 25, 1565−1579

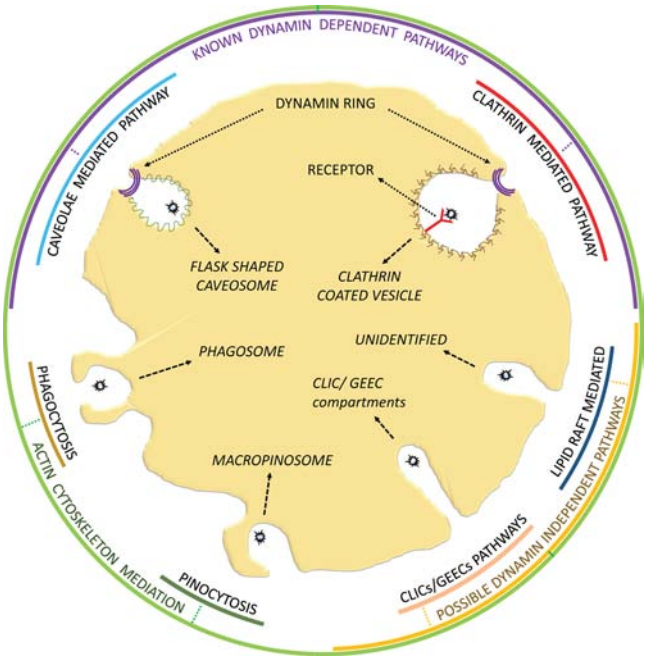

Figure 1. Overview of the endocytic pathways involved in internalization of molecules in a mammalian cell. In general, receptor based internalization of molecules involves clathrin machinery.

icity toward gastrin releasing peptide receptors (GRPR) under in vivo conditions.[29,30] GRPR is overexpressed in a variety of human cancers, such as prostate, breast, and lung cancers.[31] We have previously demonstrated that BBN conjugated gold nanoparticles (AuNPs) have both in vitro and in vivo affinity for the GRPR.[32,33] Based upon this information, we hypothesized that BBN conjugated AuNPs internalize in GRPR expressing human cancer cells using a receptor-mediated endocytosis (clathrin) mechanism, and subsequently release from endosomes to the cytosol. To validate this hypothesis, we synthesized a library of BBN conjugated 45-nm-sized gold nanocages (AuNCs) to study the mechanistic interactions between GRPR and AuNC-BBN conjugates.

Pioneering efforts by Xia and co-workers have resulted in the synthesis and biomedical applications of polyvinylpyrrolidone (PVP) capped AuNCs.[34,35] As demonstrated in several studies, AuNCs belong to one of the most interesting smart classes of porous nanomaterials and have potential applications in both therapy and diagnosis of cancer.[20,36] Porous space within AuNCs enable higher payloads and controlled delivery of drugs to a desired organ or cellular site.[37] Upon delivery, strong absorption of high intensity near-infrared radiation (NIR) by the AuNCs can be utilized to release the drug selectively to cancer cells.[38,39] To achieve therapeutic success, it is vital that AuNCs possess the ability to selectively recognize and internalize within cancer cells. We designed bombesin peptide functionalized AuNCs to address this critical need. Herein, we report results of the following studies: (i) synthesis, stability, and in vitro characteristics of AuNC-BBN conjugates; (ii) GRPR affinity of AuNC-BBN conjugates; and (iii) mechanism and cellular trafficking of AuNC-BBN conjugates in human prostate tumor cells. Although our present studies elucidate endocytosis mechanisms that have broader implications, our experiments were geared toward prostate cancer. According to the American cancer society, prostate cancer accounts for nearly 29% (i.e., 241 740 estimated cases) of the total male cancer cases in the US for the year 2012 alone.[40] A previous study involving 36 human prostate tumor patients demonstrated that a large majority (83%) of the patients showed very high density of GRPR (>1000 dpm/mg tissue) in tumor regions.[31] Hence, there exists a significant research and clinical interest in developing biomolecules to target GRPR that are overexpressed in human prostate tumor. It is worth noting that BBN peptide has shown very high in vivo affinity for targeting GRPR in prostate tumors.[23] Several studies have established that the BBN peptide (agonist) selectively targets GRPRs and internalize via the receptor mediated pathway.[22,30] In the present study, AuNCs are surface conjugated to BBN peptide via a modified dithiol linkage to transform the nanocages to be specific to GRPRs. Owing to the specificity of BBN and the unique properties of nanocages, the combination of both would serve as a desired platform for developing novel nanodelivery systems. Thus, studies of the endocytic route and the intracellular trafficking of bombesin functionalized nanocages (AuNC-BBN) in human cancer cells can provide deeper insight and assist in the development of efficient therapeutic nanopharmaceuticals with low toxicity.

SYNTHESIS AND CHARACTERIZATION

Synthesis of Bombesin Coated Gold Nanocages. We prepared two different kinds of AuNC-BBN conjugates (see Scheme 1): (i) AuNC-BBN-PVP nanocage surface coated with

Scheme 1. Schematic Illustration of the Synthesis of Bombesin Conjugated Gold Nanocages

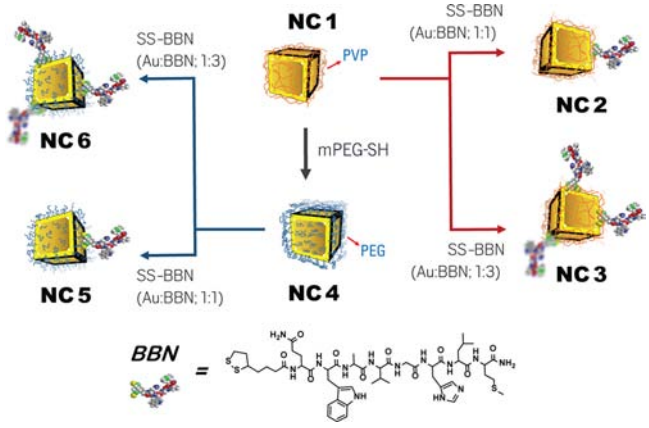

both bombesin peptide and PVP (NC2 and NC3), wherein NC2 and NC3 differ in concentrations of BBN molecules present on the cage surface; and (ii) AuNC-BBN-PEG nanocage surface coated with bombesin peptide and PEG (NC5 and NC6), wherein NC5 and NC6 differ in concentrations of BBN coatings on the surface. AuNC-PVP (NC1) was synthesized as previously reported in the literature.[34,41] The PVP on the surface was partially displaced using different amounts of thioctic acid-BBN peptide to obtain NC2 and NC3. In a similar fashion, PVP on NC1 was totally displaced using thiol-PEG-750 to obtain NC4. Subsequently, thiol-PEG-750 was partially displaced by different amounts of thioctic acid-BBN to obtain NC5 and NC6 (see Experimental Methods section for details on synthesis). All six nanocages exhibited characteristic UV−visible NIR absorption at 700−750 nm confirming the cage shaped nanoconjugates. Zeta potentials (ζ) of precursors NC1 and NC4 showed a negative value, whereas BBN substitution on the surface resulted in significant

dx.doi.org/10.1021/bc500295s | Bioconjugate Chem. 2014, 25, 1565−1579

Table 1. Physicochemical Properties of Gold Nanoconjugates

conjugate code	conjugate name	Au:BBN	ζ (mV)	hydrodynamic size (nm)	IC_{50} PC3 (ng/mL)
NC1	AuNC-PVP	Control	−35.2	100.2	NA
NC2	AuNC-BBN-pvp	1:1	−11.9	105.8	32.6 ± 9
NC3	AuNC-BBN-pvp 0.2 mg BBN/mg NC3 (HPLC)	1:3	25.4	111.7	5.8 ± 3
NC4	AuNC-PEG	Control	−39.7	88.0	NA
NC5	AuNC-BBN-peg	1:1	15.9	150.6	32.9 ± 17
NC6	AuNC-BBN-peg 0.13 mg BBN/mg NC6 (HPLC)	1:3	36.3	142.4	15.6 ± 4

change in the ζ-potential (Table 1). Increase in ζ-potential reflected a higher amount of BBN peptide conjugated on the surface. The sizes of the synthesized cages were determined using both DLS and TEM methods (Table 1; Figure S4 and S7 (b) in Supporting Information). DLS measurements indicated size increase from ∼100 nm (NC1) to ∼112 nm (NC3) upon BBN substitution.[42] Size increase was markedly higher in the case of PEGylated cages, where the size increased from ∼88 nm (NC4) to ∼142 nm (NC6).[43] Further, TEM studies showed AuNCs are homogeneous, with a wall thickness of ∼7 nm (see Figures S4 and S5 in Supporting Information). A thin layer of gold is clearly visible on the face of the cages, and porous spaces are visible as white spots. Xia and co-workers have shown that AuNCs contain silver atoms within the interior.[44] Indeed, our quantification studies using flame atomic absorption spectroscopy (FAAS) showed that the gold−silver ratios in AuNCs is ∼6:1. Furthermore, to confirm the presence of BBN on the surface, we carried out cyanide digestion of NCs to liberate the surface bound BBN peptide, and subsequently identified and quantified the peptide using both UV−visible spectroscopy and HPLC analysis. In these experiments, gold atoms in NCs were reacted with cyanide (CN^-) to form water-soluble $Au(CN)^{2-}$ ions.[45,46] As a result, the surface bound BBN peptide was released into the solution and identified by monitoring its (i) UV-absorption at 280 nm and; (ii) retention time of 11.9 min in HPLC analysis (see Figures S8−S13 in Supporting Information for details). Both the analytical methods correlate with each other. For example, 1 mg of NC3 contained 0.22 mg of BBN on the surface as determined by UV−visible spectroscopy and 0.20 mg of BBN using HPLC analysis. In a similar fashion, NC6 contained 0.15 mg (UV−visible spectroscopy) and 0.13 mg (HPLC) of bombesin peptide on the surface (see Table 1).

RESULTS AND DISCUSSION

Receptor Affinity of Bombesin Coated Gold Nanocages. To evaluate the receptor affinity of bombesin functionalized AuNCs toward GRPRs, we performed the following experiments using human prostate tumor (PC3) cells. The rationale for choosing PC3 cells is based on the fact that they exhibit higher GRPR density (∼44 000 sites/cell) on the surface compared to other human cancer cells.[47] Nanoconjugates (NC1, NC4, NC3, and NC6) were treated with fixed PC3 cells for 2 h and analyzed using dark field microscopy, wherein fixed cells have active receptors on the surface and all of the components inside the cells are inactive or dead. Both NC1 and NC4 serve as controls since there are no BBN peptides attached to their surface. A significant number of NC3 and NC6 were observed to be attached to the surface of cancer cells (see Figure 2g−l) in which the gold signals (yellow spots) correspond to NCs as proven by hyperspectral analysis (see Figure S14 in Supporting Information). Such an attachment is expected because receptors are present on the surface, and the BBN peptide conjugated NC3 and NC6 have natural affinity to bind to these receptors. As expected, the controls NC1 and NC4 did not show any preferential localization on the surface of the cells. Based on this experiment, it is evident that both NC3 and NC6 recognize the GRPRs present on the cancer cells. In order to quantify the GRPR affinity of NCs, we performed *in vitro* competitive displacement cell binding assays (IC_{50}) on PC3 cells using radiolabeled ^{125}I-Tyr^4-BBN. In this experiment, we used nanocages with varying levels of BBN attached to the surface, anticipating that NCs containing fewer BBN peptides on the surface should show low affinity—that is, high IC_{50} values. Indeed, IC_{50} values for NC2, NC3, NC5, and NC6 were 32.6 ± 9 ng/mL, 5.8 ± 3 ng/mL, 32.9 ± 17 ng/mL, and 15.6 ± 4 ng/mL, respectively (Figure 3 and Table 1). As expected, a higher BBN peptide ratio to gold surface leads to lower IC_{50} values,

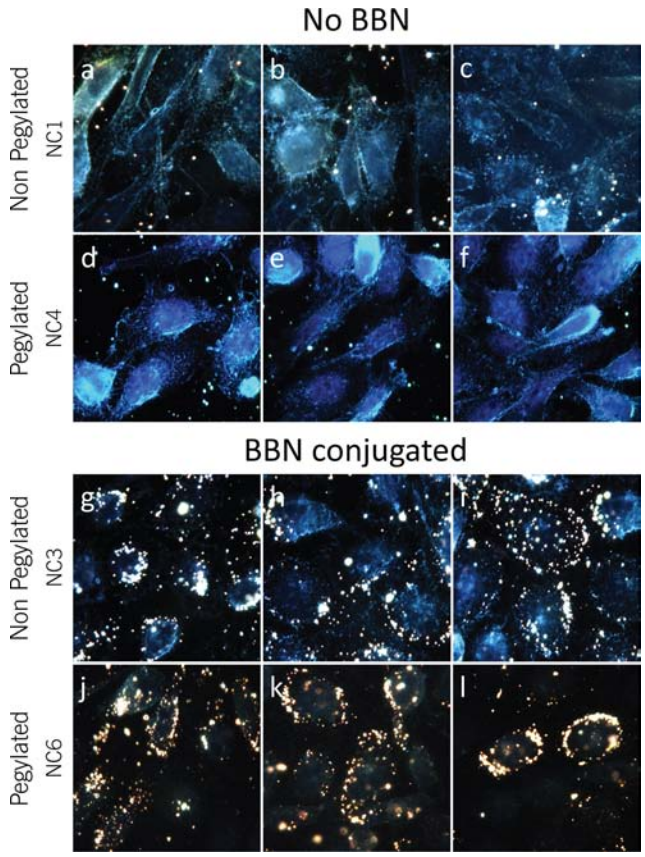

Figure 2. PC3 cells were fixed before treating with nanoconstructs. GRP receptors present on the cell surface would be active even after fixing the cells. Bombesin conjugated nanoconjugates recognize these receptors on the cell surface and bind to them. Representative dark field backscattering images of fixed PC3 cells after treatment with the following nanoconjugates: (a−c) NC1; (d−f) NC4; (g−i) NC3; and (j−l) NC6.

dx.doi.org/10.1021/bc500295s | Bioconjugate Chem. 2014, 25, 1565−1579

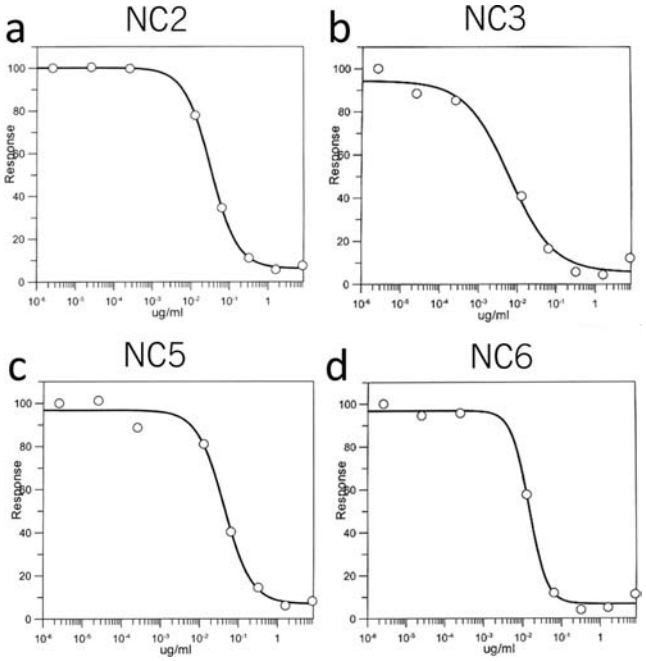

Figure 3. Inhibition of ^{125}I-Tyr^4-BBN binding to GRP receptors overexpressed in human prostate tumor cell line by (a) NC2, (b) NC3, (c) NC5, and (d) NC6. All nanoconjugates exhibited characteristic sigmoid curves for the displacement of radiolabeled bombesin conjugates from cancer cells with increasing concentrations of nanoconstructs. Both NC3 and NC6 showed excellent IC_{50} values compared to lower bombesin peptide containing NC2 and NC5, respectively.

and to increased binding affinity with PC3 cells. It is worth noting here that NC3 showed a relatively lower IC_{50} value (higher affinity) when compared with NC6. This data further confirms the estimated BBN amounts analyzed from our cyanide digestion experiment.

Cellular Internalization Pathway of Bombesin Coated Gold Nanocages. Cells streamline their metabolic processes for maximum efficiency by creating various pathways through which they distinguish different types of signals, energy resources, and recycle components required for self-sustenance.[48,49] These pathways are either receptor (specific) or nonreceptor (nonspecific) processes (Figure 1). Receptor specific pathways in cells utilize adaptor proteins to recruit molecules such as clathrins or caveolins (to compartmentalize incoming molecules after receptor binding); these are referred to as clathrin-mediated endocytosis (CME) or caveolae mediated pathway.[50,51] On the other hand, nonreceptor pathways are known to be based on macropinocytosis or phagocytosis.[52] AuNC-BBN conjugates could utilize either one of the pathways for internalization. In order to understand the mechanism of internalization, we utilized well-known inhibitors to block specific pathways. The techniques used to analyze and quantify are discussed in the following sections.

Energy Dependent or Independent Pathway? To evaluate whether or not the cellular internalization of bombesin-coated AuNCs are mediated by energy dependent endocytosis, we incubated NC3 or NC6 with PC3 cells at 4 °C and monitored their uptake using optical microscopy. If the internalization process is energy dependent, then a decreased uptake of AuNCs should be observed. Indeed the uptake of AuNCs within the cells was significantly reduced at 4 °C when compared with that of internalization at 37 °C (see Figure S19 in Supporting Information). This result confirms that active endocytic pathways were involved in the transport of AuNC-BBN cages within the tumor cell. It is worth noting here that a similar decrease in uptake of biomolecule-coated gold nanorods was observed at 4 °C in HeLa cells, normal bronchial epithelial cells, and primary adult stem cells.[18,53] Yet, interestingly, Casibang et al. have shown that bombesin peptide analogs show decreased cellular uptake at 4 °C in GRPR expressing cancer cells.[54] Taken together, it is evident that AuNC-BBN conjugates internalize through an energy dependent pathway in PC3 cells similar to other bombesin analogs and biomolecule conjugated nanorods.[32] As NC3 shows higher dynamic-aggregation in cell media, results do not truly reflect mechanistic characteristics. Further experiments utilized NC6 due to its higher stability toward aggregation in cell media. Therefore, we chose to focus our further investigation on NC6 rather than NC3 (see Figures S15 and S16 in Supporting Information).

Clathrin/Caveolae or Macropinocytosis/Phagocytosis? It has been established that clathrin or caveolae based pathways are dynamin dependent while macropinocytosis or phagocytosis are not.[55,56] Therefore, we investigated the dynamin pathway dependency of NC6 to internalize within the cells and thereby differentiate between these pathways. Dynamin plays a key role in vesicular scission of a clathrin or a caveolar pit, at the

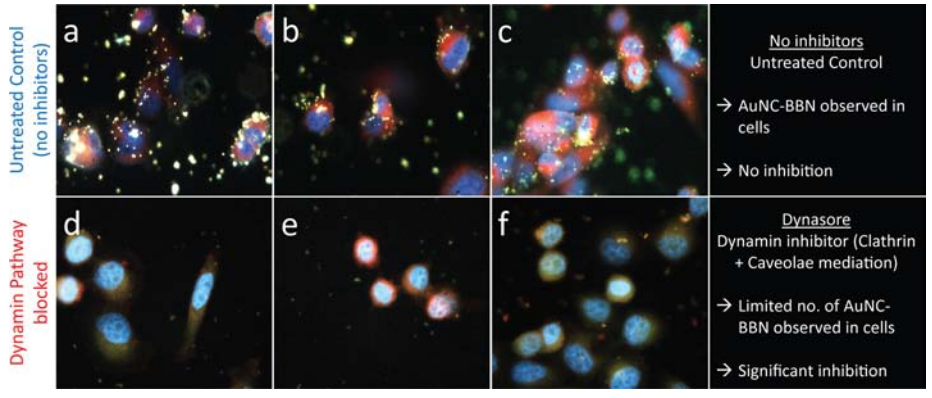

Figure 4. Bombesin conjugated nanocage NC6 requires dynamin for entry in PC3 cells. NC6 was treated with PC3 cells in the presence and absence of a dynamin inhibitor. Representative dark field images (100× magnification, stained with DAPI and CellMask, oil immersion) of cells in the (a–c) absence and (d–f) presence of dynamin inhibitor.

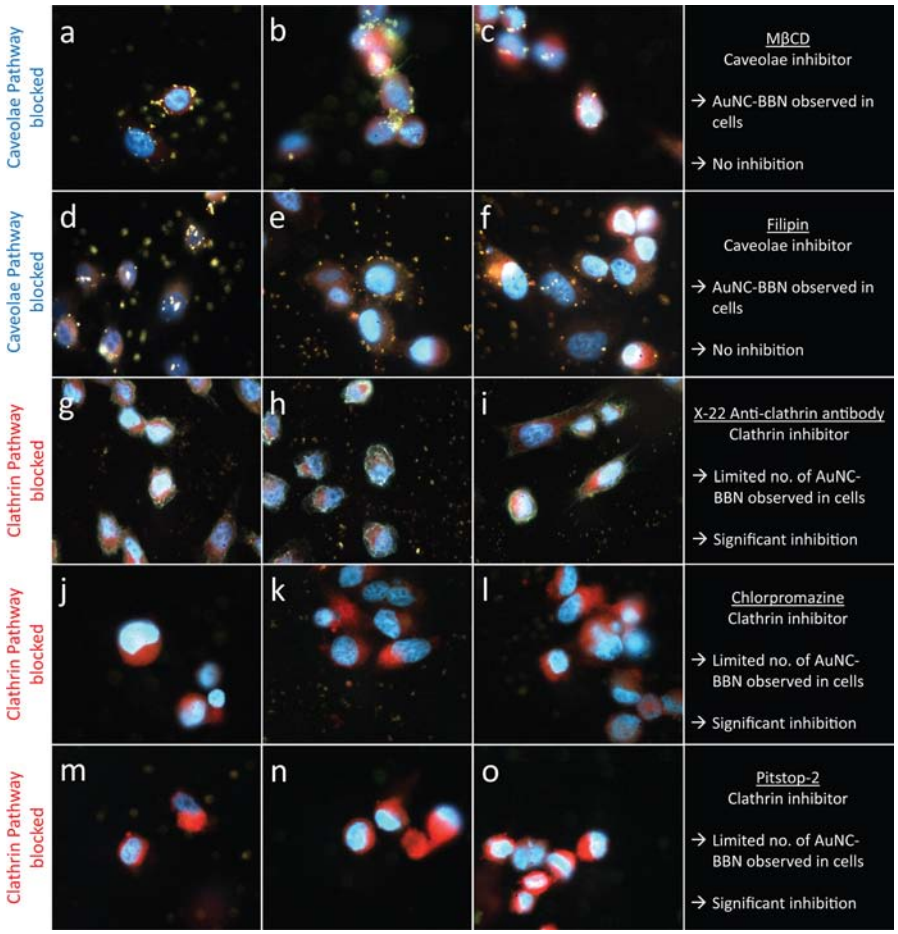

Figure 5. Caveolae inhibitors MβCD and filipin did not influence the internalization of NC6 in PC3 Cells, whereas clathrin inhibitors anti-clathrin antibody, chlorpromazine and pitstop-2 significantly influence the internalization. Representative dark field images (100× magnification, stained with DAPI and CellMask, oil immersion) of cells treated with caveolae inhibitors (a–c) MβCD; (d–f) Filipin; and clathrin inhibitors (g–i) X-22 anti-clathrin antibody; (j–l) Chlorpromazine; and (m–o) Pitstop-2.

cellular membrane, for subsequent budding and internalization.[57,58] In order to evaluate whether NC6 follows a dynamin pathway, we used dynasore hydrate to block dynamin function, thereby arresting clathrin and caveolae mediated endocytosis.[59,60] In the present study, we treated PC3 cells with dynasore, followed by treatment with NC6 for 4 h. Cells were subsequently monitored using dark field back scattering images. Gold signals in the cells provided the measure of internalization. Indeed, in comparison to the untreated cell (Figure 4a–c), a significant decrease in gold signals was observed for internalization of NC6 in PC3 cells treated with dynasore (Figure 4d–f). These results indicate that internalization follows the conventional trend of dynamin dependent internalization pathway (i.e., clathrin or caveolae pathway) and independent of phagocytosis and macropinocytosis. Similar results were obtained by Yang and co-workers to explain a dynamin and clathrin dependent uptake of nanoclusters.[61] Of interest to the present study, Rotello and co-workers have shown that AuNPs surface functionalized with nontargeting cationic ligand moiety enter into nonmalignant cells via a dynamin dependent, caveolae pathway.[12] We performed further mechanistic evaluation to interpret whether AuNC-BBN internalizes by either a caveolae or clathrin pathway.

Clathrin or Caveolae? As a next step, we independently blocked caveolae and clathrin pathways in the cell using well-known inhibitors and studied the internalization characteristics of AuNC-BBN (NC6). The caveolae pathway functions via formation of pits along the membrane supported by cholesterol dependent caveolin networks.[62,63] For inhibiting the caveolae pathway, we used cholesterol depletors such as methyl-β-cyclodextrin (MβCD) or filipin.[64−67] PC3 cells were pretreated with inhibitor followed by AuNC-BBN conjugate for 4 h. Subsequently, the cells were imaged using dark field microscopy, and the images confirmed moderate accumulation of nanoconjugates in cell cytoplasm (Figure 5a–f). This observation established that AuNC-BBN uptake in PC3 cells is via a caveolar independent process. These results can be interpreted as a clathrin dependent process as proposed in similar inhibition work by Zhao et al.[68] Furthermore, in order to prove CME as the major endocytic pathway, we blocked the clathrin machinery in the cancer cells and studied the internalization of AuNC-BBN. During the CME process, AP-2, amphimysin, and clathrin serve as adaptors to form vesicular clathrin coated cages.[57,69] Blocking the adaptors using inhibitors such as anti-clathrin antibodies, chlorpromazine (AP-2 redistributor), or Pitstop-2 (amphimysin interferer) destabilize the formation of clathrin cages and subsequently arrest CME.[67,70] In other words, arresting CME in cells should result in decreased internalization of AuNC-BBN conjugates. PC3 cells were independently pretreated with inhibitor followed by AuNC-BBN treatment for 4 h. The treated cells show significant decrease in AuNC-BBN uptake as shown in

dx.doi.org/10.1021/bc500295s | *Bioconjugate Chem.* 2014, 25, 1565−1579

Figure 5g–o. These images showed large number of cells devoid of AuNCs. Thus, these results established that AuNC-BBN conjugates enter into cells using CME.

Subsequently, for quantification of AuNC-BBN internalized in PC3 cells we utilized neutron activation analysis (NAA) technique. Using this technique, the amount of gold present in the cells was estimated. Specifically, NC6 internalized in cells pretreated with inhibitors (clathrin and caveolae) was compared with untreated cells. As expected, clathrin inhibitors reduced AuNC-BBN conjugate internalization in the cells by 20% (see Figure S21 in Supporting Information). However, due to nonspecific adsorption of AuNCs on the substrate the results were erroneous. To circumvent the problem of nonspecific binding of AuNCs, we pretreated the substrate with poly-L-lysine before seeding the cells; subsequently, the cells were treated with NC6. After treatment, cells were sorted using flow cytometry (see Figure S22 in Supporting Information). Cells that were internalized with NC6 were analyzed using NAA technique (see Figure S23 in Supporting Information). As shown in Figure S23, cells that were pretreated with clathrin inhibitors (anti-clathrin antibody and Chlorpromazine) showed significant reduction in internalization. On comparison with untreated cells, we observe that there is a reduction of ~60% (in the case of antibody) and ~85% (in the case of chlorpromazine) in internalization of NC6. These results further independently validate that bombesin conjugated nanocages internalize via clathrin mediated endocytosis. We also utilized dark field backscattering microscopy for quantification of internalized NC6 in PC3 cells. In this microscopic technique, a given field of view enabled visualization of multiple cells. AuNC-BBN nanoaggregates present within the cell showed gold signals (bright yellow spots). Using the field of view, the average number of nanoaggregates present in 200 cells was used to compare the accumulation of AuNC-BBN in cells (see Experimental Methods section for details). The very nature of having a huge sample size (i.e., number of cells on substrate) allowed us to average and quantify aggregates as a basis of comparative internalization. The quantification study revealed a decrease in total equivalent uptake of 85.97% and 85.90% for clathrin inhibitors (chlorpromazine and pitstop-2) compared to untreated controls. In the colocalization study using X-22 anti-clathrin antibody, nanocage uptake decreased by 81.23%. On the other hand, caveolar inhibition showed only a meager 23.85% reduction in uptake compared to untreated controls (Figure 6). Earlier reports showed similar reduction in free BBN peptide uptake for clathrin blocking studies using fluorescence analysis.[22] These results show that AuNC-BBN's internalization in cells depends on clathrin machinery. Other endocytic transit routes such as caveolae (lipid transport) and novel uninvestigated pathways may endocytose in parallel at low transit sustenance.[71] These types of internalizations can be due to cross-linking or charge based nanoparticle coupling effects. This effect increases the total package size ($x > 300$ nm) and allows a cell to take up the package via other routes, since clathrin mediation is size dependent, where x is the average nanocluster diameter.[72] This behavior has also been attributed to uptake wrapping times where NP surface energy is supposed to play a key role.[73,74]

Cellular Trafficking of Bombesin Coated Gold Nanocages. In order to understand the endocytic mechanism and intracellular fate of nanocages, we utilized transmission electron microscopy (TEM). TEM images provided valuable

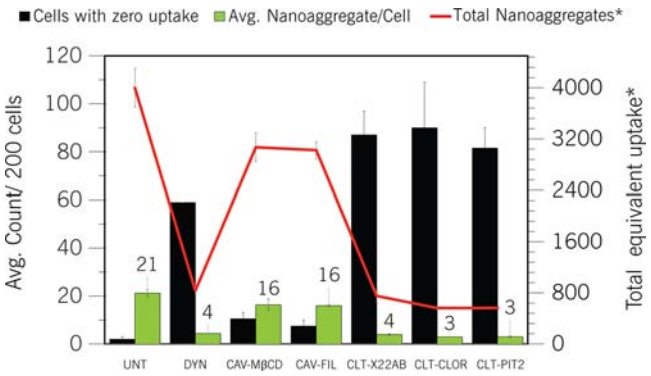

Figure 6. Quantitative analysis of NC6 internalized in PC3 cells in the presence and absence of caveolae and clathrin inhibitors using optical microscopy technique (dark field fluorescence illumination). The legend indicates the following: (UNT) untreated; (DYN) dynamin pathway blocked with Dynasore; (CAV-MβCD) caveolae pathway blocked with methyl-β-cyclodextrin; (CAV-FIL) caveolae pathway blocked with filipin; (CLT-X22AB) clathrin pathway inhibited during colocalization by anti-clathrin antibody; (CLT-CLOR) clathrin pathway blocked with chlorpromazine; (CLT-PIT2) clathrin pathway blocked by Pitstop-2. The nanoparticles in two hundred cells were monitored and quantified. Each visible gold signal, i.e., nanoaggregate, was approximated as one unit. PC3 cells treated with clathrin inhibitors internalize fewer AuNCs.

subcellular location of nanoconjugates that aid in explaining the endocytic steps involved in CME. The seven major steps (represented in Figure 7–13) are outlined as follows.

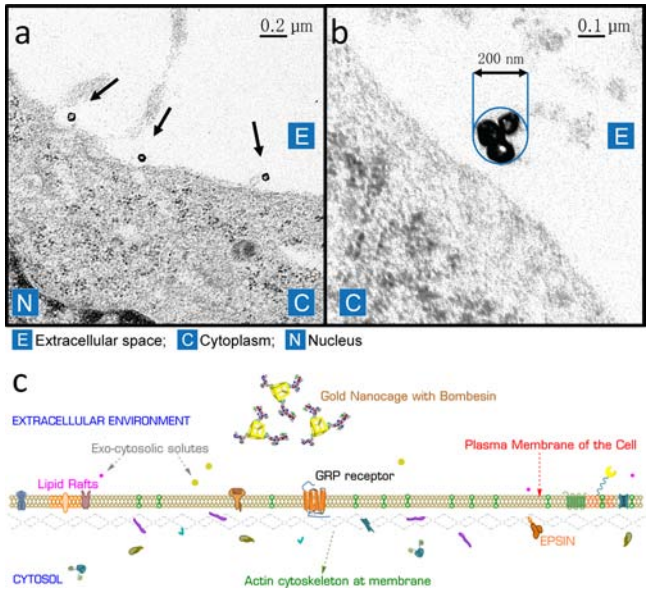

Figure 7. (a,b) TEM images of NC6 in a prebinding cellular environment (see arrows). (c) Schematic representation of the prebinding cellular environment. (Molecules depicted in all subsequent steps can be identified using a glossary available in the Supporting Information; Figure S28.)

Step 1, Prebinding. A prebinding environment is a crucial step for determining the method of internalization. AuNC-BBN can present itself in monomeric, dimeric, or multimeric (aggregated) forms to the cellular surface. If AuNC-BBN utilizes CME as a process of internalization, its dynamical aggregates should not exceed the 300 nm size limit.[72] Indeed,

dx.doi.org/10.1021/bc500295s | Bioconjugate Chem. 2014, 25, 1565–1579

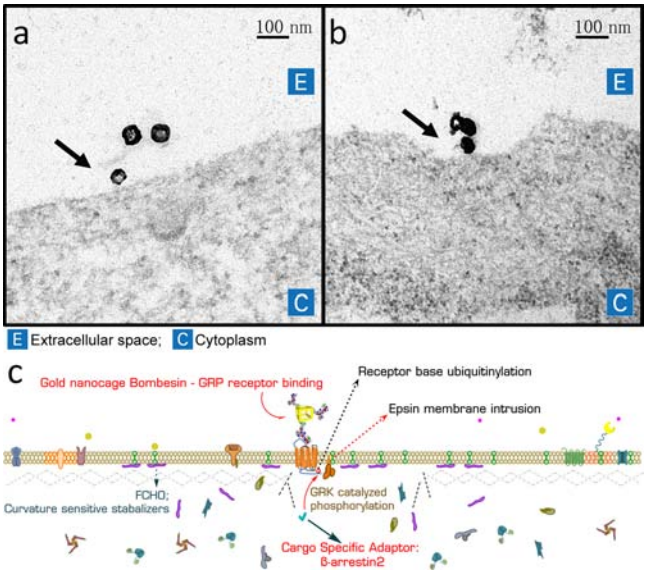

Figure 8. (a,b) Binding of NC6 with GRP receptors on PC3 cancer cells is shown in TEM images. The TEM images show postbinding signal cascade and membrane intrusion environment within cells (see arrows). (c) Schematic representation of the above environment depicting the important events.

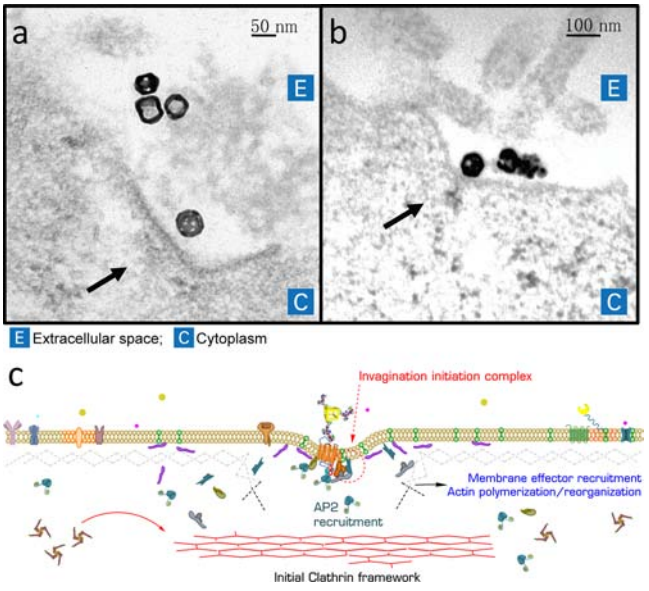

Figure 9. (a,b) Binding of NC6 results in curving of the cellular membrane as observed in TEM images. Thickening of membrane is observed at these sites (see arrows). (c) Schematic representation of effector recruitment needed for initial curvature.

TEM images of the prebinding environment show that NC6 presents itself to a cancer cell in the form of monomeric or trimeric AuNC nanoclusters which do not exceed the 300 nm size limit (Figure 7). Therefore, the CME process would be a predominant mode of internalization.

Steps (2) Post-Binding Signal Cascade and (3) Membrane Curving. These steps trigger many molecular changes within cells which cannot be captured by TEM imaging (Figure 8). It is expected that after AuNC-BBN binds to GRPR present on the cell surface, the $\beta\gamma$-trimeric subunit of the G-protein is phosphorylated by the G-protein receptor kinase (GRK).[75] Subsequently, activation leads to GRPR C-terminal exposure

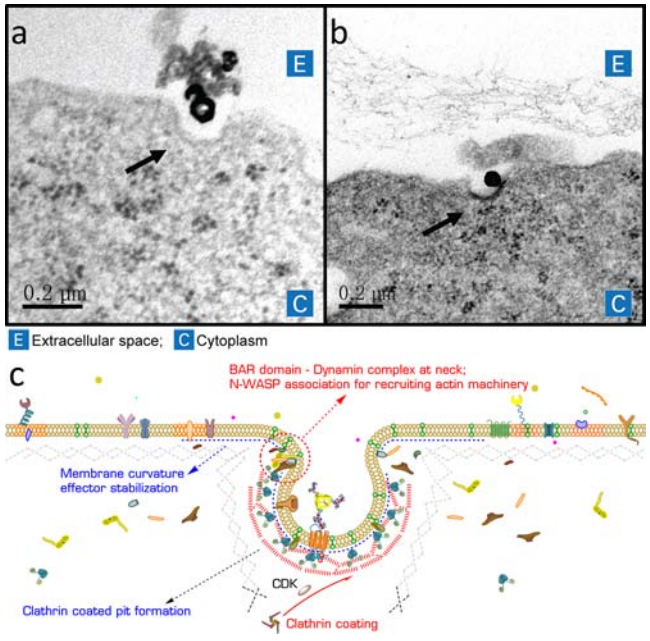

Figure 10. Formation of clathrin coated pits in the cellular membrane is characteristic of clathrin mediated endocytosis of NC6. (a,b) Before internalization of nanocage the membrane pit formation is observed in TEM images along the cellular membrane (labeled with arrows). (c) Schematic representation of the primary invagination and clathrin cage formation (scaffolding complexes lining the pit are now shown as a blue dotted line for simplicity).

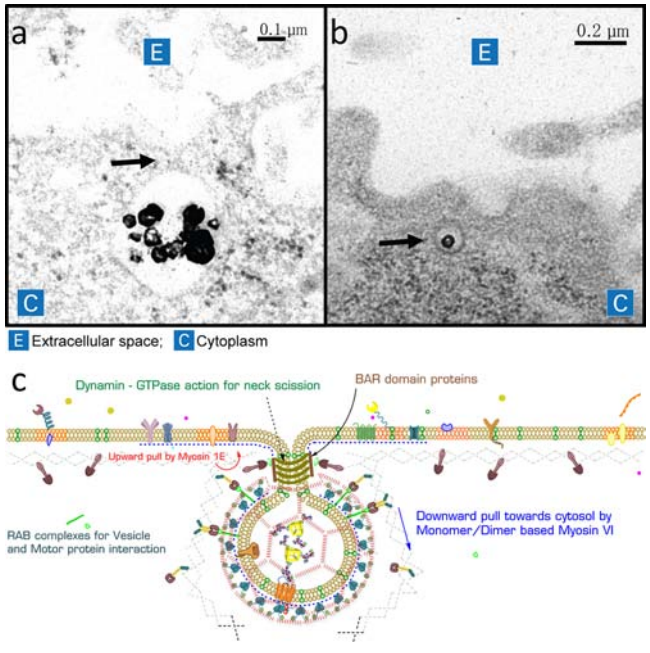

Figure 11. Transformation of clathrin pits to nascent vesicles. (a,b) TEM images showing pit closure and characteristic clathrin coated vesicles (CCVs). The arrow in part (a) indicates the point of tubulation where the dynamin ring would be present and (b) CCV containing a single nanocage. (c) Schematic representation of scission and budding operations involved in CME.

and arrestin dependent regulation for incoming nanocages.[76,77] Once such signals have been communicated, the first and most significant event is the formation of positive curvature toward cytosol in the plasma membrane near the receptor.[42,44]

dx.doi.org/10.1021/bc500295s | Bioconjugate Chem. 2014, 25, 1565−1579

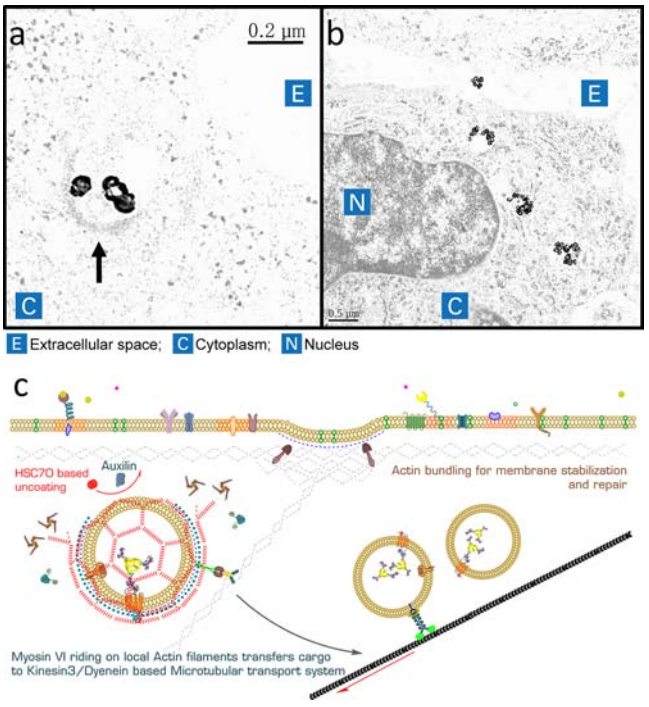

Figure 12. Trafficking of nanocages within cells is controlled by the method of endocytosis. NC6 conjugates were internalized via CME process. (a,b) TEM images show uncoating of clathrin coated vesicles (labeled with arrow) and their transport within cells as early endosomes. (c) Schematic representation of uncoating and vesicular transport of nascent internalized vesicle.

Membrane curving would reflect a postbinding scenario as evident in TEM images (Figure 9). It is believed that, after binding, Epsin associates with Eps15 and intersectins to form a primary invagination complex leading to widespread induction for membrane curving of the cell.[58,78] The curved membrane triggers clathrin and AP2 to form the cage within that area of binding.[66] It is worth noting here that we studied the internalization of NC6 in the presence of AP2 redistributing agent (chlorpromazine).[79] Chlorpromazine causes redistribution of AP2 near the membrane by directing them to endosomes.[80] Due to lack of AP2 concentration, clathrin cages did not form, thereby reducing endocytic trafficking of NC6 at the membrane (Figure 5). In addition we selectively blocked action of clathrin molecules by pretreating cells with anti-clathrin antibodies (X-22). As expected, internalization of NC6 was reduced within cells (Figure 5).

Steps (4) Pit Formation and (5) Vesicular Scission. These steps confirm that NC6 internalizes via CME into cells.[81] The uptake of AuNCs via CME was confirmed by characteristic clathrin coated pit formations along the cellular membrane as shown in TEM images (Figure 10). For purposes of simplifying the schematic representations, the membrane effectors and scaffolding complexes lining the pit are now represented as a blue dotted line over the pit area as depicted in Figure 10. It is also evident from the TEM images that the neck of the pit starts narrowing (becoming tubulated) toward the membrane leading to vesicular budding of clathrin coated vesicles or CCVs (Figure 11). The neck narrowing is known to be specific with a dynamin associated CME process. In previous sections, we have shown that inhibition of dynamin (using "dynasore") resulted in poor internalization of AuNC-BBN within cells. Furthermore, we see similar inhibition when cells were pretreated with pitstop-2 that interferes with amphimysin, which closely associates with dynamin.[70] Altogether, the results confirm a dynamin dependent uptake for AuNC-BBN.

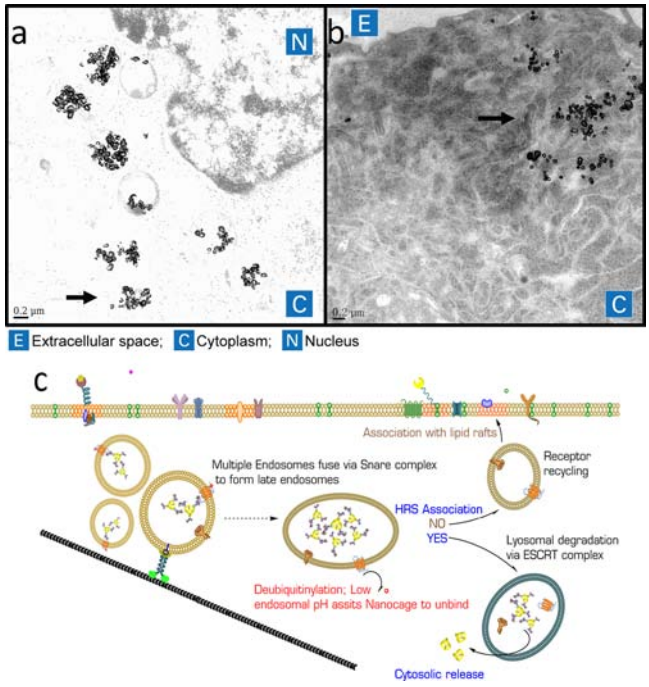

Figure 13. Release of nanocages from lysosome is an important event in trafficking. (a,b) TEM images showing NC6 unbinding within lysosomes. The arrows in the figure indicate AuNCs present in cytoplasm after their eventual lysosomal release. (c) Schematic representation of the endosomal receptor recovery and lysosomal degradation process.

Steps (6) Clathrin Uncoating leading to Endosomal Transport, and (7) Lysosomal Accumulation and Release. Immediately after scission of AuNC-BBN containing vesicles, the clathrin coat is uncoated to prevent it from impeding its transport to early endosomes. Vesicular transport is a well-known process and its role in CME has been demonstrated earlier.[82−84] Figure 12 shows budded vesicles with half hemispherical thickness (clathrin uncoated vesicle). Moreover, nanocages in nascent vesicles seem to be firmly tethered to the inner wall (see Figures S26 (a) and S27 (a) in Supporting Information). This tethering displays the "AuNC-BBN-GRPR" binding strength on the inner wall following the pit formation and intake. This characteristic pattern follows through the early endosome and late endosomal accumulations where the endosomal pH is supposed to be similar. A noticeable increase in AuNC particle number within late endosomes due to fusion of multiple early endosomes is seen in TEM images (Figure 12). Further, late endosomes sort into lysosomes via ESCRT complex association.[85−87] Figure 13a also highlights freely floating nanocages in accumulated lysosomes confirming that AuNC-BBN disassembles from the GRPR. Le Roy and others have explained this mechanism in terms of deubiquitination of receptors.[85,88,89] Deubiquitination occurs in order to signal cargo processing components that the receptor has finished serving its purpose, after which they are recycled or degraded depending on HRS association.[88−90] Eventually AuNC-BBNs would be subjected to lysosomal release as evident in Figure 13b. Previous studies have shown that peptides that undergo

dx.doi.org/10.1021/bc500295s | Bioconjugate Chem. 2014, 25, 1565−1579

receptor mediated internalization within cells degrade in lysosomes.[91] After degradation, the receptors are recycled to surface membrane. Bombesin peptide undergoes similar degradation and the GRP receptors are expressed back to the cellular surface.[92] In the present study, bombesin containing NC6 degrades in lysosomes and enhances the release of nanocages to cytoplasm. According to Chu et al., one other governing factor which can lead to release from lysosomes to cytoplasm can be attributed to anisotropic shape of nanocages.[93] This event can lead to eventual rupture of lysosomal membrane and cytosomal accumulation of nanocages. As explained in Figures 7−13, CME is a highly dynamic process with recruitment of various biomolecules including adaptors, operators, constructors, and motor proteins working in tandem. Our studies have established that nanocages can be utilized to track the modulation of biomolecules that are involved in endocytic pathway within the cells. Altogether this clearly proves that AuNC-BBN uptake depends on CME. It is important to note that Juliano and co-workers also showed BBN's dependency via CME, therefore indicating no loss in peptide specificity when conjugated to a passive delivery nanocarrier (AuNCs).[22]

CONCLUSIONS

A library of bombesin conjugated gold nanocages was synthesized and characterized using conventional analytical techniques. In vitro experiments revealed that AuNC-BBN conjugates have high affinity toward GRPRs that are overexpressed on the PC3 cell surface. These selective recognition characteristics could be significantly important in designing targeted therapeutic nanodelivery systems for treating tumors. Similar to BBN peptide, AuNC-BBN internalized predominantly via a CME process in GRPR expressing human cancer cells. This data confirms that the intrinsic targeting characteristic of bombesin is retained even after conjugating with AuNCs. Most importantly, this study demonstrates that surface ligands play a crucial role in internalization and subsequent trafficking of nanoparticles. Furthermore, electron microscopy studies confirm stepwise molecular events of interaction of AuNC-BBN with tumor cells. This mechanistic insight opens the door for future targeted delivery of peptide conjugated nanoparticles to oncology applications.

EXPERIMENTAL METHODS

Synthesis of NC1. Silver nanocubes were used as the starting template for gold nanocage synthesis. Nanocubes were synthesized by a polyol reduction process using silver nitrate to form silver seeds, as published by Xia and co-workers.[41] Briefly, the slightly modified procedure is given as follows: 60 mL ethylene glycol was taken in a (3-necked) 250 mL round-bottom flask and heated to 150 °C under constant stirring around 350 rpm for 50 min. Argon gas at 20 kPa was introduced through a nozzle above the solution for 10 min. After initial argon flushing, the remaining reaction was performed under argon gas at 10 kPa. 0.7 mL of sodium hydrosulfide dissolved in ethylene glycol (3 mM) and 15 mL of polyvinylpyrrolidone (PVP) dissolved in ethylene glycol (20 mg/mL; MW 55 000) were then added in quick succession. After 8 min, 5 mL of $AgNO_3$ dissolved in ethylene glycol (48 mg/mL) was quickly added into the reaction solution. Within moments of addition of $AgNO_3$, a light yellow solution was observed and after 20 min it turned to green ochre. The reaction was stopped at this moment and cooled in an ice bath for 5 min. The reaction mixture was centrifuged and the pellet was washed once with acetone and 6 times with water to remove excess PVP. Finally, washed silver nanocubes were dissolved in 10 mL water. Gold nanocages were then synthesized by a previously reported procedure.[34,94] Briefly, the slightly modified procedure is given as follows: AuNCs were synthesized by titrating prepared silver nanocubes with $HAuCl_4$ in the presence of PVP as a stabilizer. Initially, 10 mL of PVP dissolved in water (2 mg/mL; MW 55 000) was taken in a (2-necked) 300 mL round-bottom flask and 10 mL prepared silver nanocubes was then pipetted into the flask. Flask was heated to 100 °C under constant stirring around 400 rpm for 5 min. $HAuCl_4$ (0.9 mM) was injected at a rate of 45 mL/h using a syringe pump until the reaction mixture gave a UV−vis absorbance maximum at 750 nm. After addition, the reaction mixture was cooled in an ice bath for 5 min. The solution was centrifuged (7000*g*) for 20 min. Supernatant was discarded and the pellet was washed with water containing 400 μL of NH_4OH to remove AgCl from the product.[94] Subsequently, the solution was centrifuged 6 times with water to remove excess PVP (10 000*g* for 10 min). Final purified product NC1 was further concentrated and freeze-dried for storage at −20 °C.

Synthesis of NC2 and NC3. Five mg of NC1 was suspended in 2 mL of water in a vial by sonicating for 10 min, and kept at constant stirring conditions around 200 rpm. Thiolated BBN (MW 1129) dissolved in 2 mL methanol was added according to 1:1/1:3 Gold-BBN molar ratio (unless otherwise indicated, all experiments utilized the 1:3 ratio). After 12 h incubation at room temperature, the centrifuged pellet was washed twice with methanol to remove free bombesin, followed by 6 washings in water. Final products (AuNC-BBN-PVP) were labeled NC2 (1:1 ratio) and NC3 (1:3 ratio). Products were further concentrated, freeze-dried, and stored at −20 °C.

Synthesis of NC5 and NC6. Five mg of NC1 in 2 mL of water was sonicated for 10 min. To this solution, thiolated PEG (MW 750) dissolved in 2 mL water was added according to 1:3 Gold-PEG molar ratio. After 12 h incubation at room temperature, NC4 was obtained and washed 6 times in water and subsequently incubated with modified thiolated Bombesin peptide (Lipoic-QWAVGHLM-NH_2) to bind to gold surface. Two mL of NC4 was taken in a vial and kept at constant stirring conditions around 200 rpm. Thiolated BBN (MW 1129) dissolved in methanol was added according to 1:1/1:3 Gold-BBN molar ratio (unless otherwise indicated all experiments utilized the 1:3 Au:BBN ratio). After 12 h incubation at room temperature, suspension was centrifuged at 10 000*g* for 10 min, and the pellet was washed twice with methanol to remove free BBN, followed by 6 washings with water. Final products (AuNC-BBN-PEG) were labeled NC5 (1:1) and NC6 (1:3). Products were further concentrated, freeze-dried, and stored at −20 °C.

Characterization of AuNCs. Nanocages synthesized in this study were characterized using UV−vis spectroscopy, TEM, DLS, and NTA measurements. As described in the synthetic protocol, AuNCs are synthesized using silver nanocube templates which have UV−vis absorption at 410 nm shown in Figure S1 (see Supporting Information). The silver nanocubes are reduced with gold salt and etched to increase porosity. Resulting AuNCs have a broad UV−vis absorption at the NIR region as shown in Figure S2 (see Supporting Information). As the templates were cubic in nature, nanocages

are also hollow cubic structures as confirmed by TEM images (Figure S3 and Figure S4 in Supporting Information). We estimated the thickness of the surface of the AuNCs to be ∼7.0 nm. The face of the cube contains gold atoms with porous space inside the cage (Figure S4 in Supporting Information). Although their core sizes appear similar in TEM there is a noticeable change in hydrodynamic size and ζ-potentials (Table S1 in Supporting Information). The homogeneous size of AuNCs is corroborated using nanoparticle tracking analysis (NTA) shown in Figure S5 (see Supporting Information).

Estimation of Bombesin. To identify and confirm the presence of bombesin on the surface of the nanoparticles after conjugation, AuNCs were dissolved in methanol and digested using sodium cyanide. This digestion process detaches bombesin molecules from the surface of nanoparticles. Subsequently, bombesin peptide was identified by its UV−vis absorption peak at 280 nm. Bombesin peptide was unaffected in the presence of NaCN as established in our control reaction. For this experiment, 0.4 mg/mL SS-BBN dissolved in methanol was taken as the control. It is important to note that SS-BBN treated with saturated NaCN methanol solution showed no effect in UV−vis spectral absorption. Each nanoconjugate (equal concentration) were separately taken in two vials. One vial had pure methanol as solvent taken as control while the other had NaCN dissolved methanol. After 5 min of treatment, UV−vis measurements were performed and the results were compared with control study. UV−vis measurements were taken for two ranges: 230−380 nm and 220−950 nm to show BBN peak and AuNC digestion, respectively. In order to estimate BBN, NC3 and NC6 with known dry weight and known gold amounts were digested for 5 min in NaCN solution, and further centrifuged two times in order to obtain a supernatant free of any remaining precipitates. Bombesin peptide's standard concentration curves were prepared for estimation using spectroscopy and HPLC techniques.

UV−vis spectra and TEM of NC3 and NC6 are shown in Figure S7 (see Supporting Information). Bombesin peptide was identified using UV−vis spectroscopy and HPLC. In UV−vis spectroscopy, SS-Bombesin showed a peak at around 280 nm (see Figure S8 in Supporting Information). In HPLC, SS-BBN showed a retention time of 11.9 min (CH_3CN-H_2O gradient system) and monitored using UV detector (280 nm) as shown in Figures S12 (see Supporting Information). The presence of SS-BBN in the supernatant was observed after digestion of nanocage NC3, while for its control NC1 (devoid of SS-BBN on surface) no corresponding absorption peak was observed after nanocage digestion as shown in Figure S9 (see Supporting Information). This data confirms the presence of unbound BBN after AuNC digestion. Similarly the peak for SS-BBN was visible after NC6 digestion, while for its control NC4 (devoid of SS-BBN on surface) no corresponding peak was observed after nanocage digestion. Results are shown in Figure S10 (see Supporting Information). Concentration curves were recorded in order to estimate bombesin amounts in NC3 and NC6 as shown in Figure S11−S13 (see Supporting Information).

Cell Culture. PC3 human prostate carcinoma cells (ATCC, USA) were grown in RPMI 1640 medium (obtained from Gibco BRL, Grand Island, NY). The media was supplemented with 4.5 g/L D-glucose, 25 mM Hepes, 0.11 g/L sodium pyruvate, 1.5 g/L sodium bicarbonate, 2 mM L-glutamine, 10% heat-inactivated fetal bovine serum (Atlanta Biologicals, USA), and 1% penicillin/streptomycin antibiotic solution. Cells were cultured in a humidified atmosphere of 95% air and 5% CO_2 at 37 °C (Thermo Scientific, USA).

In Vitro Stability Studies and MTT Assay. The stability of NC3 and NC6 was investigated in biologically relevant solutions with respect to time. Nanoconjugates (800 μL) were suspended in 6 different solutions (200 μL), namely, 0.9% sodium chloride, 0.5% bovine serum albumin, 0.5% human serum albumin, 0.5% cysteine, 0.2 M histidine, and 1× phosphate buffer saline. Stability of nanoconjugates was monitored using UV−vis absorption of gold nanocages vs time for 1 and 24 h periods, respectively. Both NC3 and NC6 appear to have high stability within the 24 h time period as shown in Figure S15−S16. As a whole, PEGylated particles appear to be more stable and show higher solubility. Visible aggregates of NC3 were observed in the vial after dissolution. In sharp contrast, NC6 remained stable during the study period.

For in vitro toxicity assays, MTT tests were performed for all nanoconjugates (NC1−NC6) to investigate the cytotoxicity in PC3 cells (5×10^5 cells/well; 37 °C). Cells at exponential growth phase were seeded in a flat bottom 96-well polystyrene coated plate and incubated for 12 h at 37 °C. Various concentrations of nanoconjugate solutions (NC1−NC6) in media were prepared: 2.5 μg/mL, 5 μg/mL, 10 μg/mL, 25 μg/mL, and 50 μg/mL. Each sample was tested in triplicates for statistical analysis. After 24 h incubation, 10 μL per well MTT (stock solution 5 mg/mL 1× PBS) (ATCC, USA) was added and kept for 4 h, and the formazan crystals so formed were dissolved in 100 μL detergent/solubilizing buffer. The plates were kept for 2 h in the dark at 25 °C to dissolve all crystals, and the intensity of developed color was measured using a Biotek Epoch plate reader operating at 570 nm wavelength. Wells with complete medium, nanoparticles, and MTT, but without cells, were used as blanks. Untreated cells were considered 100% viable. Intensities were then represented as dosage vs viability response charts. Cytotoxicity studies performed using MTT assay show relative cell viability of 60% for higher doses up to 50 μg/mL. It is evident from Figure S17 (see Supporting Information) that nanoconjugates with bombesin seem to be relatively toxic compared to BBN devoid counterparts. NC1 and NC4 controls show gradual decrease in viability, while NC2, NC3, NC5, and NC6 plateaus to 70−80% viability for all concentrations.

Determination of IC_{50} Values. Half maximal inhibitory concentration (IC_{50}) values were determined for NC2, NC3, NC5, and NC6. Results were derived by radioactive assays in PC3 cells by comparing specificity of nanocage to that of radioactive bombesin analogue ^{125}I-Tyr^4 BBN (GRPR specific peptide) in a competitive binding assay. Approximately 30 000 cells were incubated at 37 °C for 40 min under 5% CO_2 in the presence of 20 000 cpm ^{125}I-Tyr^4-bombesin (2200 Ci/mmol). Along with the radioactive BBN analogue, nanoconjugates were coincubated in PC3 cells with increasing dosage. After incubation, the reaction medium was aspirated, and cells were washed three times with cold RPMI 1640 modified buffer. Cell bound radioactivity was then measured by a Packard Riastar γ-counter. IC_{50} values were calculated using GraphFit 4.0 graphing software to plot dosage response curves where values were represented in μg/mL. Each sample was tested in triplicate for statistical analysis as shown in Figure S29 (see Supporting Information). Final values were calculated in ng/mL.

Hyperspectral Imaging. Optical microscopy for nanocage cellular internalization studies was performed using the Cytoviva dark field fluorescence microscope. In the image, gold signals were observed for AuNCs. As a first step, we proved that gold signals correspond to light scattered from the surface of AuNCs. To prove that the gold signals (or yellow spots) were AuNCs, we matched the hyperspectral profile of AuNCs with and without cells over a glass coverslip used for microscopy. AuNCs have a characteristic UV−vis absorption at the ∼790 nm due to surface plasmon resonance. However, they also have a characteristic reflectance in the red band of the visible spectrum. In a dark field microscopic study, AuNCs illuminate in the red band, and the scattered light can be recorded as a hyperspectral profile. Therefore, spectral profiles for AuNCs on an empty glass slide and AuNCs in cells were compared for a match. Indeed, we see similar profiles for bombesin conjugated AuNCs with and without cells as shown in Figure S14 (e and f) (see Supporting Information). The spectral profile data confirm that the gold signals (bright yellow spots) in cell slides are AuNCs. Spectral library was constructed by assembling the scattering characteristics of multiple nanocages. The spectral profile for AuNCs inside the cells was similar to that of control AuNCs. For these experiments, we used the following protocol: 2 μL of dilute bombesin conjugated AuNCs was sandwiched between a clean glass slide and a coverslip. After drying for 10 min in a 40 °C hot air oven, the slide was focused under the dark field microscope at 100×. Using ENVI imaging software, spectral profiles for AuNCs were recorded. Similarly, microscope slides containing nanoconjugate incubated cells were also viewed and a spectral library was made, and later matched with the control.

Pathway Blocking Study. In order to investigate the endocytosis of nanoconjugates in cells, the conjugates were analyzed for both caveolae and clathrin mediated endocytosis. All nanoconjugates (NC1−NC6) were selectively studied under the following regime: (a) cells without any inhibitors; (b) cells blocked for clathrin mediated endocytosis; (c) cells blocked for caveolae mediated endocytosis; (d) all modes of endocytosis blocked for cells treated at 4 °C. For all these experiments, PC3 cells were grown in 6-well plates (5×10^5 cells/well). Treatment concentrations in each well for clathrin blocking study were 10 μM chlorpromazine (affects AP2 distribution and clathrin lattice assembly) and 2 μM cytochalasin D (assists blocking actin function). Treatment concentrations in each well for caveolae blocking study were 5 mM methyl-β-cyclodextrin (blocks lipid raft mediation via cholesterol depletion) and 100 μM amiloride (blocks macropinocytosis via submembranous acidification). All samples were treated with inhibitors for 30 min followed by nanocage treatment (50 μL of 0.2 mg/mL) for 2 h at 37 °C. For energy dependent study (blocks all modes of endocytosis), cells were incubated for 30 min at 4 °C, followed by nanocage treatment (50 μL of 0.2 mg/mL) for 2 h at 4 °C conditions. For additional controls, PC3 cells were not incubated with any nanocages. After 1 h treatment, cells were washed to remove unbound nanocages, and microscopic slides were prepared with DAPI nuclear stain. Endocytosis in PC3 cells were then observed using Cytoviva dark-field imaging (100× oil).

Dark field imaging was utilized for investigating the cellular internalization of nanocages at both 37 and 4 °C. High concentrations of NC3 and NC6 were internalized in PC3 cells at 37 °C; however, the internalization was drastically reduced under 4 °C (see Figure S19 (a−d) in Supporting Information). This result indicates AuNCs cellular uptake process to be based on an energy dependent pathway. To understand the endocytic pathway response to surface coating, nanoconjugates NC1, NC3, NC4, and NC6 were investigated for possible associations with caveolae and clathrin transport mechanisms. As shown in Figure S20 (g and h) (see Supporting Information), NC3 and NC6 did not internalize after the clathrin pathway was blocked. In contrast, NC1 intake is affected by blocking the caveolae pathway as seen in Figure S20 (a) (see Supporting Information). The figure also indicates that PEGylated particles do not internalize within the time frame of incubation (see Figure S20 (b and f) in Supporting Information).

Further detailed experiments were carried out to elucidate the mechanism of cellular internalization of NC6. In this study, we selectively blocked certain pathways that are required for trafficking into cells. Initially a live control study was established followed by a dynamin pathway blocked study. After a decrease in uptake was found in dynamin blocked cells, clathrin mediated and caveolae mediated endocytosis regimes were studied in PC3 cells. Internalization and subsequent accumulation were analyzed using Cytoviva dark field imaging for NC6. A known number of PC3 cells (5×10^5 cells/well) were seeded in 6-well plates. NC6 was subjected to seven experiments: (a) live control without any inhibitors; (b) dynamin pathway blocked cells using dynasore hydrate; (c) colocalization with 3 μg/mL X-22 anti-clathrin antibody; (d) two experiments for blocking clathrin pathway using chlorpromazine and pitstop-2; and (e) the other two experiments for blocking caveolae pathway using methyl-β-cyclodextrin and filipin. Treatment concentrations in each well for dynamin blocking study was 80 μM dynasore hydrate, while for clathrin blocking study they were 20 μM chlorpromazine and separately 25 μM pitstop-2. Treatment concentrations in each well for caveolae blocking study were 5 mM methyl-β-cyclodextrin and separately 5 μM filipin. After 30 min inhibitor treatment, inhibitor concentrations were halved in each well followed by NC6 (10 μL of 1 mg/mL) treatment per well. After 4 h incubation at 37 °C, the resulting cells were washed to remove unbound nanocages, and microscopic slides were prepared with DAPI nuclear stain and CellMask Deep Red plasma membrane stain. All treatments were carried out in serum free media.

Colocalization Study. In order to inhibit clathrin mediated endocytosis, X-22 anti-clathrin antibodies were colocalized with NC6 in PC3 cells. The antibodies were purified by passing through a Zeba Micro spin desalting column to remove any preservatives. The modified method for antibody internalization in live cells is described below.[95,96] First, cells were incubated with PBS for 2 min at 37 °C, followed by incubation with ice cold PBS for another 2 min. Cells were then incubated with permeabilization buffer (0.01% Tween 20 in 1× PBS at pH 7.6) for 1 min. The cells were washed with cold 1× PBS 3 times, followed by antibody treatment in serum free media at 37 °C. Cells were allowed to internalize antibody for 30 min followed by nanoconjugate treatment as explained in previous sections.

Neutron Activation Analysis. Neutron activation analysis (NAA) was utilized to quantify cytoplasmic accumulations of nanocages. In this study, nanoconjugates (NC1, NC3, and NC6) that were internalized within cells after blocking clathrin mediated or caveolae mediated endocytosis were analyzed using NAA. For these experiments, known numbers of PC3 cells (4.25×10^5 cells/well) were seeded in 6-well plates. Treatment

concentrations in each well for clathrin blocking study were 10 μM chlorpromazine and 2 μM cytochalasin D. Treatment concentrations in each well for caveolae blocking study were 5 mM methyl-β-cyclodextrin and 100 μM amiloride. For gold internalization control, cells were not incubated with gold nanocages. After 30 min inhibitor treatment, PC3 cells were treated with the respective 50 μL gold nanocage solution to achieve a gold concentration of 13.35 ppm/well. After 4 h incubation at 37 °C, resulting cells were washed, dislodged, and stored as cell pellets at −20 °C for NAA analysis for measuring varying levels of gold with respect to internalization in samples. Results shown in Figure S21 are represented as comparative percentages of gold (ppm). Each sample was performed in triplicate. The results show that both NC3 and NC6 internalize less (~20%) when the clathrin pathway is blocked compared to caveolae pathway. Nonspecific binding of AuNCs on substrate led to erroneous results. To prevent nonspecific accumulation of AuNCs, multiple washes using PBS or acidic buffers were performed. The results did not yield any desirable outcome. Such problems are quite common in the literature.[97]

To overcome the problem of nonspecific binding a separate experiment was performed. Substrates were coated with poly-L-lysine to minimize nonspecific binding while flow cytometry was utilized to separate cells (see Figures S22 and S24 in Supporting Information). The following samples were examined: (a) untreated control - without any inhibitors; (b) colocalization with 3 μg/mL X-22 anti-clathrin antibody; (c) pretreatment with clathrin inhibiting chlorpromazine. Results are presented as percentage accumulation of gold (ppm) and corroborated with data obtained with microscopy analysis (see Figure S23 and S30 in Supporting Information; see Figure S31 and Table S4 for statistical analysis). All treatments were carried out in serum free media.

Prevention of Nonspecific Binding. NC1−NC6 showed high nonspecific binding to cell plate substrates and glass coverslips. For reducing this binding, 2 mL 0.01% poly-L-lysine solution was incubated on the substrate surface in sterile conditions under UV light for 2 h. Solution was then removed using a vacuum pump and substrate was rinsed once using sterile cell grade water. Poly-L-lysine coated wells/coverslips were then allowed to air-dry in sterile conditions for 4 h under UV light. After drying, plate wells/coverslips were used for cell seeding. Poly-L-lysine, a positively cationic polymer, was used to change the substrate surface charge and increase effective steric hindrance. The polymer is noncytotoxic and did not reduce the cell adhesion at low concentrations. Substrates with no coating showed very high nonspecific binding (see Figure S24 (a and b) in Supporting Information). In contrast, coating reduced nonspecific binding significantly (see Figure S24 (c and d) in Supporting Information).

Quantification of NC6 in Cells Using Optical Microscopy. Two hundred cells from each slide were recorded during the process in order to quantify an average population of cells. The study was conducted in duplicate for statistical analysis. The study included a live control, dynamin pathway blocked experiment (DYN-BLOCK, effectively blocking both clathrin and caveolae mediation) using dynasore, caveolae blocking using methyl-β-cyclodextrin (CAV-MβCD), caveolae blocking using filipin (CAV-FIL), clathrin blocking using X-22 anti-clathrin antibody (CLT-X22AB), clathrin blocking using chlorpromazine (CLT-CLOR), and clathrin blocking using pitstop-2 (CLT-PIT2). Individual cells were analyzed for NC6 uptake as shown in Table S2 (see Supporting Information). Data from duplicate experiments were collected for analysis and averaged (see Table S3 in Supporting Information). Furthermore, we depicted the stages in a series of endocytic representations within the manuscript. The molecules illustrated in these steps can be identified with a key glossary shown in Figure S28 (see Supporting Information).

■ ASSOCIATED CONTENT

Supporting Information

Materials, Instrumentation, Abbreviations, Supplementary discussion, as well as Figures S1−S31 and Tables S1−S4. This material is available free of charge via the Internet at http://pubs.acs.org.

■ AUTHOR INFORMATION

Corresponding Author

*E-mail: kannanr@health.missouri.edu.

Notes

The authors declare no competing financial interest.

■ ACKNOWLEDGMENTS

R.K. acknowledges the Michael J. and Sharon R. Bukstein Faculty Professorship endowment on Cancer Research for financial support. Authors also acknowledge funding from MU iCATS Faculty Innovator Award, Fast Track Economic Development Award, Coulter Translational Program Bridge Funding award, and Mizzou Advantage award. The project described was also supported in part by Award Number 1I01BX001699 and a Research Career Scientist Award (TJH) from the Biomedical Laboratory Research and Development Service of the VA Office of Research and Development. The authors thank Dr. Richard Madsen, Professor of Statistics, for assistance in statistical analysis.

■ REFERENCES

(1) Brigger, I., Dubernet, C., and Couvreur, P. (2002) Nanoparticles in cancer therapy and diagnosis. *Adv. Drug Delivery Rev. 54*, 631−651.

(2) Davis, M. E., Chen, Z. G., and Shin, D. M. (2008) Nanoparticle Therapeutics: An Emerging treatment modality for cancer. *Nat. Rev. Drug Discovery 7*, 771−782.

(3) Bhattacharyya, S., Khan, J. A., Curran, G. L., Robertson, J. D., Bhattacharya, R., and Mukherjee, P. (2011) Efficient delivery of gold nanoparticles by dual receptor targeting. *Adv. Mater. 23*, 5034−5038.

(4) Lynch, I., Cedervall, T., Lundqvist, M., Cabaleiro-Lago, C., Linse, S., and Dawson, K. A. (2007) The nanoparticle-protein complex as a biological entity; a complex fluids and surface science challenge for the 21st century. *Adv. Colloid Interface Sci. 134−135*, 167−174.

(5) Fleischer, C. C., and Payne, C. K. (2012) Nanoparticle surface charge mediates the cellular receptors used by protein-nanoparticle complexes. *J. Phys. Chem. B 116*, 8901−8907.

(6) Gonnord, P., Blouin, C. M., and Lamaze, C. (2012) Membrane trafficking and signaling: two sides of the same coin. *Semin. Cell Dev. Biol. 23*, 154−164.

(7) Canton, I., and Battaglia, G. (2012) Endocytosis at the nanoscale. *Chem. Soc. Rev. 41*, 2718−2739.

(8) Xu, S., Olenyuk, B. Z., Okamoto, C. T., and Hamm-Alvarez, S. F. (2013) Targeting receptor-mediated endocytotic pathways with nanoparticles: rationale and advances. *Adv. Drug Delivery Rev. 65*, 121−138.

(9) Muro, S. (2012) Challenges in design and characterization of ligand-targeted drug delivery systems. *J. Controlled Release 164*, 125−137.

(10) Lesniak, A., Salvati, A., Santos-Martinez, M. J., Radomski, M. W., Dawson, K. A., and Aberg, C. (2013) Nanoparticle adhesion to the cell

membrane and its effect on nanoparticle uptake efficiency. *J. Am. Chem. Soc. 135*, 1438−1444.
(11) Huang, C., Zhang, Y., Yuan, H., Gao, H., and Zhang, S. (2013) Role of nanoparticle geometry in endocytosis: laying down to stand up. *Nano Lett. 13*, 4546−4550.
(12) Saha, K., Kim, S. T., Yan, B., Miranda, O. R., Alfonso, F. S., Shlosman, D., and Rotello, V. M. (2013) Surface functionality of nanoparticles determines cellular uptake mechanisms in mammalian cells. *Small 9*, 300−305.
(13) Nativo, P., Prior, I. A., and Brust, M. (2008) Uptake and intracellular fate of surface-modified gold nanoparticles. *ACS Nano 2*, 1639−1644.
(14) Tsuji, T., Yoshitomi, H., and Usukura, J. (2013) Endocytic mechanism of transferrin-conjugated nanoparticles and the effects of their size and ligand number on the efficiency of drug delivery. *Microscopy (Oxford) 62*, 341−352.
(15) Bhattacharyya, S., Singh, R. D., Pagano, R., Robertson, J. D., Bhattacharya, R., and Mukherjee, P. (2012) Switching the targeting pathways of a therapeutic antibody by nanodesign. *Angew. Chem., Int. Ed. Engl. 51*, 1563−1567.
(16) Jiang, W., Kim, B. Y., Rutka, J. T., and Chan, W. C. (2008) Nanoparticle-mediated cellular response is size-dependent. *Nat. Nanotechnol 3*, 145−150.
(17) Perrault, S. D., Walkey, C., Jennings, T., Fischer, H. C., and Chan, W. C. (2009) Mediating tumor targeting efficiency of nanoparticles through design. *Nano Lett. 9*, 1909−1915.
(18) Chithrani, B. D., and Chan, W. C. (2007) Elucidating the mechanism of cellular uptake and removal of protein-coated gold nanoparticles of different sizes and shapes. *Nano Lett. 7*, 1542−1550.
(19) Bhattacharyya, S., Bhattacharya, R., Curley, S., McNiven, M. A., and Mukherjee, P. (2010) Nanoconjugation modulates the trafficking and mechanism of antibody induced receptor endocytosis. *Proc. Natl. Acad. Sci. U. S. A. 107*, 14541−14546.
(20) Chen, J., Wang, D., Xi, J., Au, L., Siekkinen, A., Warsen, A., Li, Z. Y., Zhang, H., Xia, Y., and Li, X. (2007) Immuno gold nanocages with tailored optical properties for targeted photothermal destruction of cancer cells. *Nano Lett. 7*, 1318−1322.
(21) Dixit, V., Van den Bossche, J., Sherman, D. M., Thompson, D. H., and Andres, R. P. (2006) Synthesis and grafting of thioctic acid-PEG-folate conjugates onto Au nanoparticles for selective targeting of folate receptor-positive tumor cells. *Bioconjugate Chem. 17*, 603−609.
(22) Ming, X., Alam, M. R., Fisher, M., Yan, Y., Chen, X., and Juliano, R. L. (2010) Intracellular delivery of an antisense oligonucleotide via endocytosis of a G protein-coupled receptor. *Nucleic Acids Res. 38*, 6567−6576.
(23) La Bella, R., Garcia-Garayoa, E., Bahler, M., Blauenstein, P., Schibli, R., Conrath, P., Tourwe, D., and Schubiger, P. A. (2002) A 99mtc(I)-postlabeled high affinity bombesin analogue as a potential tumor imaging agent. *Bioconjugate Chem. 13*, 599−604.
(24) Anas, A., Okuda, T., Kawashima, N., Nakayama, K., Itoh, T., Ishikawa, M., and Biju, V. (2009) Clathrin-mediated endocytosis of quantum dot-peptide conjugates in living cells. *ACS Nano 3*, 2419−2429.
(25) Antonella, A., Diego, T., and Giancarlo, M. (2013) Peptide-based targeting strategies for simultaneous imaging and therapy with nanovectors. *Polym. J. 45*, 481−493.
(26) Yao, L., Daniels, J., Moshnikova, A., Kuznetsov, S., Ahmed, A., Engelman, D. M., Reshetnyak, Y. K., and Andreev, O. A. (2013) Phlip peptide targets nanogold particles to tumors. *Proc. Natl. Acad. Sci. U. S. A. 110*, 465−470.
(27) Reubi, J. C. (2003) Peptide receptors as molecular targets for cancer diagnosis and therapy. *Endocr. Rev. 24*, 389−427.
(28) Borghouts, C., Kunz, C., and Groner, B. (2005) Current strategies for the development of peptide-based anti-cancer therapeutics. *J. Pept. Sci. 11*, 713−726.
(29) Akeson, M., Sainz, E., Mantey, S. A., Jensen, R. T., and Battey, J. F. (1997) Identification of four amino acids in the gastrin-releasing peptide receptor that are required for high affinity agonist binding. *J. Biol. Chem. 272*, 17405−17409.
(30) Ma, L., Yu, P., Veerendra, B., Rold, T. L., Retzloff, L., Prasanphanich, A., Sieckman, G., Hoffman, T. J., Volkert, W. A., and Smith, C. J. (2007) In vitro and in vivo evaluation of Alexa Fluor 680-Bombesin[7−14]Nh2 peptide conjugate, a high-affinity fluorescent probe with high selectivity for the gastrin-releasing peptide receptor. *Mol. Imaging 6*, 171−180.
(31) Markwalder, R., and Reubi, J. C. (1999) Gastrin-releasing peptide receptors in the human prostate: relation to neoplastic transformation. *Cancer Res. 59*, 1152−1159.
(32) Chanda, N., Shukla, R., Katti, K. V., and Kannan, R. (2009) Gastrin releasing protein receptor specific gold nanorods: breast and prostate tumor avid nanovectors for molecular imaging. *Nano Lett. 9*, 1798−1805.
(33) Chanda, N., Kattumuri, V., Shukla, R., Zambre, A., Katti, K., Upendran, A., Kulkarni, R. R., Kan, P., Fent, G. M., Casteel, S. W., et al. (2010) Bombesin functionalized gold nanoparticles show in vitro and in vivo cancer receptor specificity. *Proc. Natl. Acad. Sci. U. S. A. 107*, 8760−8765.
(34) Skrabalak, S. E., Au, L., Li, X., and Xia, Y. (2007) Facile synthesis of Ag nanocubes and Au nanocages. *Nat. Protoc. 2*, 2182−2190.
(35) Skrabalak, S. E., Chen, J., Au, L., Lu, X., Li, X., and Xia, Y. (2007) Gold nanocages for biomedical applications. *Adv. Mater. 19*, 3177−3184.
(36) Cang, H., Sun, T., Li, Z. Y., Chen, J., Wiley, B. J., Xia, Y., and Li, X. (2005) Gold nanocages as contrast agents for spectroscopic optical coherence tomography. *Opt. Lett. 30*, 3048−3050.
(37) Moon, G. D., Choi, S. W., Cai, X., Li, W., Cho, E. C., Jeong, U., Wang, L. V., and Xia, Y. (2011) A new theranostic system based on gold nanocages and phase-change materials with unique features for photoacoustic imaging and controlled release. *J. Am. Chem. Soc. 133*, 4762−4765.
(38) Mahmoud, M. A., Snyder, B., and El-Sayed, M. A. (2010) Surface plasmon fields and coupling in the hollow gold nanoparticles and surface-enhanced Raman spectroscopy. theory and experiment†. *J. Phys. Chem. C 114*, 7436−7443.
(39) Yavuz, M. S., Cheng, Y., Chen, J., Cobley, C. M., Zhang, Q., Rycenga, M., Xie, J., Kim, C., Song, K. H., Schwartz, A. G., et al. (2009) Gold nanocages covered by smart polymers for controlled release with near-infrared light. *Nat. Mater. 8*, 935−939.
(40) American Chemical Society (2012) Cancer facts and figures 2012, http://www.cancer.org/acs/groups/content/@epidemiologysurveilance/documents/document/acspc-031941.pdf.
(41) Zhang, Q., Cobley, C., Au, L., McKiernan, M., Schwartz, A., Wen, L. P., Chen, J., and Xia, Y. (2009) Production of Ag nanocubes on a scale of 0.1 g per batch by protecting the nahs-mediated polyol synthesis with argon. *ACS Appl. Mater. Interfaces 1*, 2044−2048.
(42) Pons, T., Uyeda, H. T., Medintz, I. L., and Mattoussi, H. (2006) Hydrodynamic dimensions, electrophoretic mobility, and stability of hydrophilic quantum dots. *J. Phys. Chem. B 110*, 20308−20316.
(43) Maldiney, T., Richard, C., Seguin, J., Wattier, N., Bessodes, M., and Scherman, D. (2011) Effect of core diameter, surface coating, and PEG chain length on the biodistribution of persistent luminescence nanoparticles in mice. *ACS Nano 5*, 854−862.
(44) Chen, J., McLellan, J. M., Siekkinen, A., Xiong, Y., Li, Z. Y., and Xia, Y. (2006) Facile synthesis of gold-silver nanocages with controllable pores on the surface. *J. Am. Chem. Soc. 128*, 14776−14777.
(45) Mei, B. C., Oh, E., Susumu, K., Farrell, D., Mountziaris, T. J., and Mattoussi, H. (2009) Effects of ligand coordination number and surface curvature on the stability of gold nanoparticles in aqueous solutions. *Langmuir 25*, 10604−10611.
(46) Podsiadlo, P., Sinani, V. A., Bahng, J. H., Kam, N. W., Lee, J., and Kotov, N. A. (2008) Gold nanoparticles enhance the anti-leukemia action of a 6-mercaptopurine chemotherapeutic agent. *Langmuir 24*, 568−574.
(47) Reile, H., Armatis, P. E., and Schally, A. V. (1994) Characterization of high-affinity receptors for bombesin/gastrin releasing peptide on the human prostate cancer cell lines Pc-3 and Du-145: internalization of receptor bound 125I-(Tyr4) bombesin by tumor cells. *Prostate 25*, 29−38.

(48) Sigismund, S., Confalonieri, S., Ciliberto, A., Polo, S., Scita, G., and Di Fiore, P. P. (2012) Endocytosis and signaling: cell logistics shape the eukaryotic cell plan. *Physiol. Rev. 92*, 273−366.
(49) Doherty, G. J., and McMahon, H. T. (2009) Mechanisms of endocytosis. *Annu. Rev. Biochem. 78*, 857−902.
(50) Rappoport, J. Z. (2008) Focusing on clathrin-mediated endocytosis. *Biochem. J. 412*, 415−423.
(51) Nabi, I. R., and Le, P. U. (2003) Caveolae/raft-dependent endocytosis. *J. Cell Biol. 161*, 673−677.
(52) Nichols, B. J., and Lippincott-Schwartz, J. (2001) Endocytosis without clathrin coats. *Trends Cell Biol. 11*, 406−412.
(53) Wang, L., Liu, Y., Li, W., Jiang, X., Ji, Y., Wu, X., Xu, L., Qiu, Y., Zhao, K., Wei, T., et al. (2011) Selective targeting of gold nanorods at the mitochondria of cancer cells: implications for cancer therapy. *Nano Lett. 11*, 772−780.
(54) Casibang, M., and Moody, T. W. (2000) (Tyr(0),Bpa(4))-Bombesin is a grp receptor agonist. *Peptides 21*, 649−653.
(55) Mayor, S., and Pagano, R. E. (2007) Pathways of clathrin-independent endocytosis. *Nat. Rev. Mol. Cell Biol. 8*, 603−612.
(56) Kumari, S., Mg, S., and Mayor, S. (2010) Endocytosis unplugged: multiple ways to enter the cell. *Cell Res. 20*, 256−275.
(57) Brodin, L., Low, P., and Shupliakov, O. (2000) Sequential steps in clathrin-mediated synaptic vesicle endocytosis. *Curr. Opin. Neurobiol. 10*, 312−320.
(58) Ungewickell, E. J., and Hinrichsen, L. (2007) Endocytosis: clathrin-mediated membrane budding. *Curr. Opin. Cell Biol. 19*, 417−425.
(59) Zhang, Z., Xiong, X., Wan, J., Xiao, L., Gan, L., Feng, Y., Xu, H., and Yang, X. (2012) Cellular uptake and intracellular trafficking of Peg-B-Pla polymeric micelles. *Biomaterials 33*, 7233−7240.
(60) Schulz, W. L., Haj, A. K., and Schiff, L. A. (2012) Reovirus uses multiple endocytic pathways for cell entry. *J. Virol. 86*, 12665−12675.
(61) Yang, L., Shang, L., and Nienhaus, G. U. (2013) Mechanistic aspects of fluorescent gold nanocluster internalization by live Hela cells. *Nanoscale 5*, 1537−1543.
(62) Parton, R. G., and Simons, K. (2007) The multiple faces of caveolae. *Nat. Rev. Mol. Cell Biol. 8*, 185−194.
(63) Hailstones, D., Sleer, L. S., Parton, R. G., and Stanley, K. K. (1998) Regulation of caveolin and caveolae by cholesterol in mdck cells. *J. Lipid Res. 39*, 369−379.
(64) Rodal, S. K., Skretting, G., Garred, O., Vilhardt, F., van Deurs, B., and Sandvig, K. (1999) Extraction of cholesterol with methyl-beta-cyclodextrin perturbs formation of clathrin-coated endocytic vesicles. *Mol. Biol. Cell 10*, 961−974.
(65) Zhang, L. W., and Monteiro-Riviere, N. A. (2009) Mechanisms of quantum dot nanoparticle cellular uptake. *Toxicol. Sci. 110*, 138−155.
(66) Schnitzer, J. E., Oh, P., Pinney, E., and Allard, J. (1994) Filipin-sensitive caveolae-mediated transport in endothelium: reduced transcytosis, scavenger endocytosis, and capillary permeability of select macromolecules. *J. Cell Biol. 127*, 1217−1232.
(67) Hussain, K. M., Leong, K. L., Ng, M. M., and Chu, J. J. (2011) The essential role of clathrin-mediated endocytosis in the infectious entry of human enterovirus 71. *J. Biol. Chem. 286*, 309−321.
(68) Zhao, S., Dai, W., He, B., Wang, J., He, Z., Zhang, X., and Zhang, Q. (2012) Monitoring the transport of polymeric micelles across mdck cell monolayer and exploring related mechanisms. *J. Controlled Release 158*, 413−423.
(69) Mousavi, S. A., Malerod, L., Berg, T., and Kjeken, R. (2004) Clathrin-dependent endocytosis. *Biochem. J. 377*, 1−16.
(70) von Kleist, L., Stahlschmidt, W., Bulut, H., Gromova, K., Puchkov, D., Robertson, M. J., MacGregor, K. A., Tomilin, N., Pechstein, A., Chau, N., et al. (2011) Role of the clathrin terminal domain in regulating coated pit dynamics revealed by small molecule inhibition. *Cell 146*, 471−484.
(71) Tolbert, L. M., and Lameh, J. (1996) Human muscarinic cholinergic receptor hm1 internalizes via clathrin-coated vesicles. *J. Biol. Chem. 271*, 17335−17342.
(72) Rejman, J., Oberle, V., Zuhorn, I. S., and Hoekstra, D. (2004) Size-dependent internalization of particles via the pathways of clathrin- and caveolae-mediated endocytosis. *Biochem. J. 377*, 159−169.
(73) Dasgupta, S., Auth, T., and Gompper, G. (2014) Shape and orientation matter for the cellular uptake of nonspherical particles. *Nano Lett. 14*, 687−693.
(74) Kievit, F. M., and Zhang, M. (2011) Cancer nanotheranostics: improving imaging and therapy by targeted delivery across biological barriers. *Adv. Mater. 23*, H217−247.
(75) Bohm, S. K., Grady, E. F., and Bunnett, N. W. (1997) Regulatory mechanisms that modulate signalling by G-protein-coupled receptors. *Biochem. J. 322* (Pt 1), 1−18.
(76) Lin, C. H., MacGurn, J. A., Chu, T., Stefan, C. J., and Emr, S. D. (2008) Arrestin-related ubiquitin-ligase adaptors regulate endocytosis and protein turnover at the cell surface. *Cell 135*, 714−725.
(77) Schumann, M., Nakagawa, T., Mantey, S. A., Howell, B., and Jensen, R. T. (2008) Function of non-visual arrestins in signaling and endocytosis of the gastrin-releasing peptide receptor (Grp receptor). *Biochem. Pharmacol. 75*, 1170−1185.
(78) McMahon, H. T., and Boucrot, E. (2011) Molecular mechanism and physiological functions of clathrin-mediated endocytosis. *Nat. Rev. Mol. Cell Biol. 12*, 517−533.
(79) Wang, L. H., Rothberg, K. G., and Anderson, R. G. (1993) Mis-assembly of clathrin lattices on endosomes reveals a regulatory switch for coated pit formation. *J. Cell Biol. 123*, 1107−1117.
(80) Subtil, A., Hemar, A., and Dautry-Varsat, A. (1994) Rapid endocytosis of Interleukin 2 receptors when clathrin-coated pit endocytosis is inhibited. *J. Cell Sci. 107* (Pt 12), 3461−3468.
(81) Quattrocchi, S., Ruprecht, N., Bonsch, C., Bieli, S., Zurcher, C., Boller, K., Kempf, C., and Ros, C. (2012) Characterization of the early steps of human parvovirus B19 infection. *J. Virol. 86*, 9274−9284.
(82) Slepnev, V. I., and De Camilli, P. (2000) Accessory factors in clathrin-dependent synaptic vesicle endocytosis. *Nat. Rev. Neurosci. 1*, 161−172.
(83) Hewlett, L. J., Prescott, A. R., and Watts, C. (1994) The coated pit and macropinocytic pathways serve distinct endosome populations. *J. Cell Biol. 124*, 689−703.
(84) Goldstein, J. L., Anderson, R. G., and Brown, M. S. (1979) Coated pits, coated vesicles, and receptor-mediated endocytosis. *Nature 279*, 679−685.
(85) Le Roy, C., and Wrana, J. L. (2005) Clathrin- and non-clathrin-mediated endocytic regulation of cell signalling. *Nat. Rev. Mol. Cell Biol. 6*, 112−126.
(86) Williams, R. L., and Urbe, S. (2007) The emerging shape of the escrt machinery. *Nat. Rev. Mol. Cell Biol. 8*, 355−368.
(87) Katzmann, D. J., Babst, M., and Emr, S. D. (2001) Ubiquitin-dependent sorting into the multivesicular body pathway requires the function of a conserved endosomal protein sorting complex, Escrt-I. *Cell 106*, 145−155.
(88) Tan, C. M., Brady, A. E., Nickols, H. H., Wang, Q., and Limbird, L. E. (2004) Membrane trafficking of G protein-coupled receptors. *Annu. Rev. Pharmacol. Toxicol. 44*, 559−609.
(89) Raiborg, C., and Stenmark, H. (2009) The Escrt machinery in endosomal sorting of ubiquitylated membrane proteins. *Nature 458*, 445−452.
(90) Ferguson, S. S. (2001) Evolving concepts in G protein-coupled receptor endocytosis: the role in receptor desensitization and signaling. *Pharmacol. Rev. 53*, 1−24.
(91) Gorden, P., Carpentier, J. L., Fan, J. Y., and Orci, L. (1982) Receptor mediated endocytosis of polypeptide hormones: mechanism and significance. *Metabolism 31*, 664−669.
(92) Swope, S. L., and Schonbrunn, A. (1987) Characterization of ligand binding and processing by bombesin receptors in an insulin-secreting cell line. *Biochem. J. 247*, 731−738.
(93) Chu, Z., Zhang, S., Zhang, B., Zhang, C., Fang, C. Y., Rehor, I., Cigler, P., Chang, H. C., Lin, G., Liu, R., et al. (2014) Unambiguous observation of shape effects on cellular fate of nanoparticles. *Sci. Rep 4*, 4495.

(94) Khlebtsov, B. N., Khanadeev, V. A., Maksimova, I. L., Terentyuk, G. S., and Khlebtsov, N. G. (2010) Silver nanocubes and gold nanocages: fabrication and optical and photothermal properties. *Nanotechnologies in Russia 5*, 454−468.
(95) Mitchell, H., Choudhury, A., Pagano, R. E., and Leof, E. B. (2004) Ligand-dependent and -independent transforming growth factor-beta receptor recycling regulated by clathrin-mediated endocytosis and Rab11. *Mol. Biol. Cell 15*, 4166−4178.
(96) Johnson, J. A., Gray, M. O., Karliner, J. S., Chen, C. H., and Mochly-Rosen, D. (1996) An improved permeabilization protocol for the introduction of peptides into cardiac myocytes. application to protein kinase C research. *Circ. Res. 79*, 1086−1099.
(97) Bagwe, R. P., Hilliard, L. R., and Tan, W. (2006) Surface modification of silica nanoparticles to reduce aggregation and nonspecific binding. *Langmuir 22*, 4357−4362.